

***Final Draft***  
**of the original manuscript:**

Chaudhary, A.-L.; Dietzel, S.; Li, H.-W.; Akiba, E.; Bergemann, N.;  
Pistidda, C.; Klassen, T.; Dornheim, M.:

**Synthesis of Mg<sub>2</sub>FeD<sub>6</sub> under low pressure conditions for  
Mg<sub>2</sub>FeH<sub>6</sub> hydrogen storage studies**

In: International Journal of Hydrogen Energy (2017) Elsevier

DOI: 10.1016/j.ijhydene.2017.02.033

Synthesis of  $\text{Mg}_2\text{FeD}_6$  under Low Pressure Conditions for  $\text{Mg}_2\text{FeH}_6$  Hydrogen Storage Studies

*Anna-Lisa Chaudhary<sup>1,\*</sup>, Sascha Dietzel<sup>2</sup>, Hai-Wen Li<sup>3</sup>, Etsuo Akiba<sup>3</sup>, Nils Bergemann<sup>1</sup>, Claudio Pistidda<sup>1</sup>, Thomas Klassen<sup>1,2</sup>, Martin Dornheim<sup>1</sup>*

<sup>1</sup> Department of Nanotechnology, Institute of Materials Research, Helmholtz-Zentrum Geesthacht, Max-Planck Strasse 1, D-21502 Geesthacht, Germany

<sup>2</sup> Department of Mechanical Engineering, Helmut Schmidt University, Holstenhofweg 85, D-22043 Hamburg, Germany

<sup>3</sup> Department of Mechanical Engineering, International Research Centre for Hydrogen Energy and WPI International Institute for Carbon Neutral Research (WPI-I2CNER), Kyushu University, Fukuoka, Japan

\* Corresponding author: [anna-lisa.chaudhary@hzg.de](mailto:anna-lisa.chaudhary@hzg.de), Ph: + 49 4152 87 2647, Fax: +49 4152 87 2636

Abstract

$\text{Mg}_2\text{FeD}_6$  is successfully synthesised with various degrees of purity using reactive ball milling and annealing under low pressure deuterium conditions to a maximum of 10 bar. The deuteride of the low cost ternary metal hydride  $\text{Mg}_2\text{FeH}_6$ , is synthesised to enable further characterisation studies such as isotopic exchange behaviour. Both on laboratory and industrial scales, keeping the pressure low reduces the need for expensive compression systems and also minimises the quantity of gas necessary for use; therefore it is important to

assess synthesis under these cost effective conditions. This is especially the case when using a specialised gas such as high purity deuterium. The maximum pressure chosen is 10 bar, to comply with the High Pressure Safety Act in Japan. This Safety Act limits the use of any gas including hydrogen and deuterium to 10 bar eliminating the use of traditional synthesis methods for  $\text{Mg}_2\text{FeH}_6$  or  $\text{Mg}_2\text{FeD}_6$  synthesis at high pressure (120 bar). Ball milling parameters such as milling times, ball to powder ratios as well as sintering times were altered to achieve improved  $\text{Mg}_2\text{FeD}_6$  yields under these low pressure conditions.

#### Keywords

hydrogen storage; magnesium iron deuteride; magnesium iron hydride; complex hydrides; low pressure

#### Introduction

Solid state hydrogen storage materials are of increasing interest for the development of complete clean green energy and storage systems. In particular, intermittent renewable energy production from the most common sources such as solar or wind, can produce hydrogen from water during times of excess load, then stored to be used with a fuel cell system at times of low production. This then allows continuous supply of energy independent of renewable source availability. Storing hydrogen as a solid within a metal matrix is a cost effective method of hydrogen storage without the need for compressing or liquefying hydrogen in the traditional storage method sense. One example of this metal matrix is the low cost ternary metal hydride  $\text{Mg}_2\text{FeH}_6$ . This material has octahedral coordination of Fe by hydrogen forming a  $\text{FeH}_6^{4-}$  anion that is surrounded by eight  $\text{Mg}^{2+}$  in a cubic  $\text{K}_2\text{PtCl}_6$  structure type configuration [1, 2].  $\text{Mg}_2\text{FeH}_6$  is stable and reversible for more than 500 cycles [3] with a storage capacity of hydrogen up to 5.47 wt. % and several publications have stated

that this material has a standard formation enthalpy of  $98 \pm 3$  [1],  $86 \pm 6$  [4] or  $77.4$  kJ/mol  $H_2$  [3]. This reaction enthalpy is comparable to that of the more commonly known metal hydride,  $MgH_2$  ( $74.06$  kJ/mol  $H_2$ ) [5], however, the advantage of  $Mg_2FeH_6$  is its significantly high volumetric capacity  $150$  kg/m<sup>3</sup> [6]. Properties such as excellent cyclability and high thermal stability also allows  $Mg_2FeH_6$  to be a promising candidate for heat storage within concentrated solar plants [3, 7-9] thus broadening its use as a practical material and highlighting the importance of material properties' characterisation.

Similarly, the deuteride,  $Mg_2FeD_6$  is an important material to synthesise and study as it can be used to further investigate hydrogen interaction properties when studying isotopic exchange behavior or neutron diffraction. One such study used neutron diffraction to analyse the absorption and desorption processes of Mg-Fe-H system and  $Mg_2FeD_6$  was used to further understand these reaction mechanisms [10].  $Mg_2FeH_6$  has also been widely combined with other hydrides to improve hydrogen properties of the overall system especially with regards to thermodynamic stability [11-14]. Examples where  $Mg_2FeD_6$  is used are the recent studies that  $Mg_2FeH_6$  used in reactive hydride composite (RHC) systems together with light weight metal borohydrides namely Li-, Na-, Mg-, Ca- and K-borohydrides [12, 15-17] have shown unique sorption behaviour different from the individual components. Chaudhary *et al.*[15] and Li *et al.* [16, 17] both reported the appearance of single step desorption behaviour with these RHC at specific anionic stoichiometries with a suggestion of hydrogen exchange contributing to this phenomenon [18]. In order to observe this hydrogen exchange,  $Mg_2FeD_6$  was synthesised and combined with the borohydride. The results showed evidence of H-D formation, either during ball milling or upon heating up to  $400$  °C, as H-D was released during the desorption process. In order to achieve such information, keeping the pressure low during raw material synthesis reduces the need for expensive compression systems and also

minimises the quantity of gas necessary for use. This is especially the case when using high purity deuterium as it is much more expensive to purchase when compared to hydrogen gas.

To date,  $\text{Mg}_2\text{FeH}_6$  and  $\text{Mg}_2\text{FeD}_6$  ( $\text{D}_2$  content 10.37 wt. %) are not produced commercially and are synthesised in individual laboratories [1, 19-23]. Mg and Fe do not exist as an intermetallic compound but can be chemically bound in the form of  $\text{Mg}_2\text{FeH}_6$  or  $\text{Mg}_2\text{FeD}_6$ , thus posing some challenges to the synthesis method. The first reported synthesis of the compounds used elemental Mg and Fe sintered at 500 °C under hydrogen or deuterium pressures between 60 and 120 bar for up to 10 days [1] however, there were significant amounts of  $\text{MgH}_2$  or  $\text{MgD}_2$  together with unreacted Mg and Fe remaining in the finished product. Subsequent studies have shown improved purity of  $\text{Mg}_2\text{FeH}_6$  when Mg was first hydrogenated to  $\text{MgH}_2$  before combining with Fe [3, 19, 21, 24]. Since this was an effective method of increasing the reaction yield, this study has extended this idea with deuterium instead of hydrogen to first synthesis  $\text{MgD}_2$  before further reacting with Fe and  $\text{D}_2$  to produce  $\text{Mg}_2\text{FeD}_6$ . The literature also showed that reactive ball milling (milling in  $\text{H}_2$  atmosphere) provided an improved synthesis route, however, evidence of  $\text{MgH}_2$ , Fe and MgO was still present. High purity  $\text{Mg}_2\text{FeH}_6$  synthesis was achieved more recently, by Polanski *et. al.*[21] as the conditions used (500 °C and 120 bar  $\text{H}_2$ ) were able to achieve a reaction yield of 94 – 97 %. The work presented here limits the synthesis pressure of both reactive ball milling and direct annealing to 10 bar, the lowest pressure reported to date for, an order of magnitude lower than the high purity work shown in Polanski *et. al.*[21]. In order to gain a high yield of product, various methods were used and compared including reactive milling in  $\text{D}_2$  atmosphere and direct pressure to ascertain which method was best whilst keeping the pressure low to a maximum of 10 bar.

For some research institutes, in particular those in Japan, the use of any gas, including hydrogen and deuterium, is limited to 10 bar due to the High Pressure Gas Safety Act (Act No. 204 June 7, 1951). This poses some synthesis challenges. This work presented here addresses some of these challenges to provide a new high-yield production route for  $\text{Mg}_2\text{FeD}_6$  under the given pressure limitations focusing on reactive planetary ball milling and the influence of synthesis parameters on the reaction yield.

### Experimental Methods

All materials for this work were handled in an argon atmosphere glovebox (Miwa, Japan) with a constant gas purifying system to reduce any risk of contamination from oxygen or water ( $\text{O}_2 < 1 \text{ ppm}$ ,  $\text{H}_2\text{O} < 1 \text{ ppm}$ ).

In order to synthesise  $\text{Mg}_2\text{FeD}_6$ ,  $\text{MgD}_2$  was first prepared from desorbed  $\text{MgH}_2$  (Alfa Aesar, 98 %), followed by deuterium  $\text{D}_2$  (Asahi sunsoshokei, 99.99 %) absorption at 10 bar. Table 1 gives the synthesis parameters used for the four batches of  $\text{MgD}_2$  that were later used to prepare  $\text{Mg}_2\text{FeD}_6$ . All batches of  $\text{MgD}_2$  were prepared by loading as supplied or ball milled  $\text{MgH}_2$  into a tube reactor where the material was heated to release  $\text{H}_2$  and later low pressure  $\text{D}_2$  was applied. Only batch 4 used ball-milled  $\text{MgH}_2$  prior to heat treatment in a planetary mill for 6 hours at 670 rpm with a ball-to-powder ratio of 20:1, by using stainless steel vials and balls.

Table 1:  $\text{MgD}_2$  synthesis conditions

Processing Step	Batch 1	Batch 2	Batch 3	Batch 4
<b>1<sup>st</sup> Step Desorption</b>				
Desorption Temperature (°C)	400	450	450	450

Vacuum Pressure (bar)	$4 \times 10^{-5}$	$4 \times 10^{-5}$	$4 \times 10^{-5}$	$4 \times 10^{-5}$
Desorption time (h)	1	4	2	4
Absorption Temperature (°C)	360	360	400	400
Deuterium Pressure (bar)	10	10	10	10
Absorption Time (h)	2	12	4	4
<b>2<sup>nd</sup> Step Desorption</b>				
Desorption Temperature (°C)	400	-	-	-
Vacuum Pressure (bar)	$4 \times 10^{-5}$	-	-	-
Desorption time (h)	1	-	-	-
<b>Absorption Conditions</b>				
Absorption Temperature (°C)	360	-	360	360
Deuterium Pressure (bar)	10	-	10	10
Absorption Time (h)	10	-	6	6

Mg<sub>2</sub>FeD<sub>6</sub> was synthesised by combining the pre-prepared MgD<sub>2</sub> with Fe (nano-powder, Sigma Aldrich, > 99%) in the stoichiometric ratio of 2:1 and milled under a reactive D<sub>2</sub> atmosphere followed by heat treatment of 10 bar D<sub>2</sub> for some batches (Table 2). Nano-sized Fe was used for the Mg<sub>2</sub>FeD<sub>6</sub> synthesis to increase the Mg-Fe interface area during the reactive milling process thus increasing reaction yield [25]. A planetary Fritsch Pulverisette 7 (Germany) mill was used for the reactive ball milling together with a pressurised stainless steel 30 ml vial with 7 mm stainless steel balls. By monitoring the pressure it was seen that there was little residual D<sub>2</sub> remaining after the different milling times shown in Table 2. After milling, batches 3 and 4 underwent further heat treatment in the tube reactor.

Table 2: Mg<sub>2</sub>FeD<sub>6</sub> synthesis parameters

<b>Processing Step</b>	<b>Batch 1</b>	<b>Batch 2</b>	<b>Batch 3</b>	<b>Batch 4</b>
MgD <sub>2</sub> Batch used	1	1	3	4

<b>Milling Conditions</b>				
Milling time (h)	6	6	12	12
Ball to powder ratio	20:1	40:1	20:1	20:1
Milling speed (rpm)	670	670	670	670
Deuterium pressure during milling (bar)	10	10	10	10
<b>Annealing conditions</b>				
Temperature (°C)	-	-	360	360
Time (h)	-	-	48	48
Deuterium pressure (bar)	-	-	10	10

A Rigaku Ultima IV X-Ray Diffractometer (XRD) (Japan) with a Cu anode ( $\lambda = 1.54051 \text{ \AA}$ ) for a  $2\theta$  range of 10 to  $80^\circ$  and a step size of  $0.01^\circ$  was used to obtain information on the crystalline phases. The data presented here show the range 20 to  $70^\circ$  to improve  $2\theta$  peak position resolution on the x-axis as there were no significant diffraction peaks beyond this range. The silicon single crystal sample holder was sealed in argon atmosphere using Scotch tape. Bruker *Diffracplus TOPAS* version 4.2 was used to analyse the XRD data obtained from the diffractometer and Crystallographic Information Files (cif) were obtained from the International Centre for Diffraction Data (ICDD) database. The fundamental parameter (FP) approach was employed within the Rietveld refinement process with all XRD data analyses to determine quantitative data and lattice parameters of the crystalline samples present. Quality of fit and uncertainties were taken from *TOPAS* in terms of the difference curve (the difference between the raw data and the calculated refinement values) and the *TOPAS* generated uncertainties reported use the bootstrap method of error determination. A point to note is that these uncertainties are for the mathematical fit of the calculated pattern to the measured pattern.

Simultaneous Differential Thermal Analysis and Thermogravimetric Analysis (DTA-TG, Rigaku Thermo - Evo II TG8120 - Canon, Japan) experiments were used to characterise the thermal properties of  $\text{MgD}_2$  and  $\text{Mg}_2\text{FeD}_6$ . The heating programme used for each sample was to heat from room temperature to 400 °C at a heating rate of 5 °C/min.

## Results and Discussion

Prior to  $\text{MgD}_2$  syntheses, XRD analyses were done on the as supplied  $\text{MgH}_2$  and the samples desorbed under the conditions given in Table 1 to confirm the purity of the material (Figure 1). The pattern from Figure 1(A) confirms the presence of  $\text{MgH}_2$  with a small amount of Mg (< 5 wt.%), consistent with the analytical data given by this manufacturer. The resultant desorption patterns Figure (B), (C) and (D) indicate that all the hydrogen was released under the conditions shown in Table 1 (desorption) with trace elements of MgO present (taken from Rietveld analysis (Table 3)). These results show that subsequent  $\text{D}_2$  absorption will not be affected by any contamination from  $\text{H}_2$ .

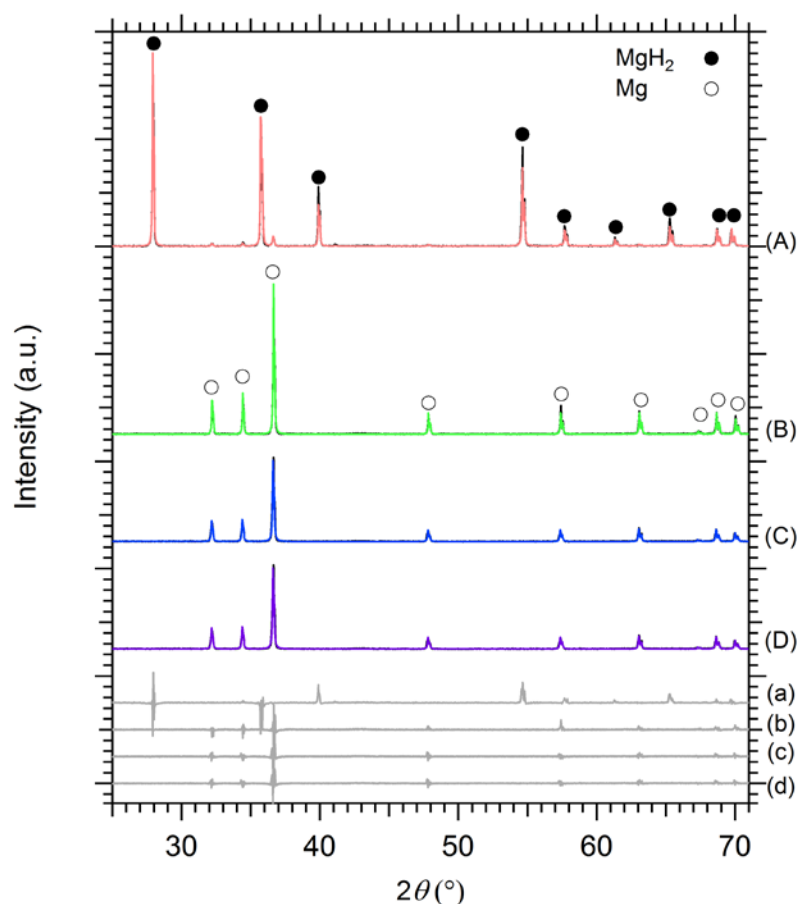


Figure 1: XRD patterns of as supplied  $\text{MgH}_2$  before and after desorption. (A) as supplied from Sigma Aldrich (B) after  $\text{H}_2$  desorption of batch 1 (C) after  $\text{H}_2$  desorption of batch 3 (D) after  $\text{H}_2$  desorption of batch 4. The grey curves, (a), (b), (c), (d), show the difference in raw data (black) and the calculated Rietveld (coloured) patterns for (A), (B), (C) and (D) respectively.

Table 3: Weight fraction and lattice parameter results from Rietveld Refinement of as supplied  $\text{MgH}_2$  as well as  $\text{MgD}_2$  after syntheses at 10 bar  $\text{D}_2$  pressure. As a reference, the lattice parameters provided in the Inorganic Crystal Structure Database (ICSD) are given.

Batch/Phase	Weight fraction observed phases (%)	Lattice Parameters (Rietveld) (Å)	Lattice Parameters (ICSD) (Å)	ICSD Number
<b><math>\text{MgH}_2</math> (as supplied)</b>				
$\text{MgH}_2$	95	a = 4.5156, c = 3.0205	a = 4.5168, c = 3.0205	#76145
Mg	5		a = 3.2094, c = 5.2103	#26624

a = 3.2097, c = 5.2100				
<b>MgH<sub>2</sub> desorbed</b>				
Mg	99	a = 3.2099, c = 5.2119		
MgO	1	a = 4.2161	a = 4.217	#9863
<b>MgD<sub>2</sub> Batch 1</b>				
MgD <sub>2</sub>	83	a = 4.5023, c = 3.0122	a = 4.5025, c = 3.0123	#18210
Mg	17			
<b>MgD<sub>2</sub> Batch 2</b>				
MgD <sub>2</sub>	77	a = 4.5034, c = 3.0125		
Mg	23			
<b>MgD<sub>2</sub> Batch 3</b>				
MgD <sub>2</sub>	60	a = 4.5023, c = 3.0120		
Mg	40			
<b>MgD<sub>2</sub> Batch 4</b>				
MgD <sub>2</sub>	98	a = 4.5032, c = 3.0124		
Mg	2			

The diffraction patterns of the D<sub>2</sub> reacted samples (conditions outline in Table 1) are given in Figure 2 and show varying degrees of reaction conversion due to the different synthesis conditions. MgD<sub>2</sub> batches 3 and 4 underwent a second absorption cycle (conditions given in Table 1) to consume any unreacted Mg after the first absorption and maximise the product yield. MgD<sub>2</sub> is structurally identical to MgH<sub>2</sub> (as indicated in Figure 1 (A) and Figure 2), however, a previous study has shown that hydrogen replaced with deuterium for some materials may result in different thermodynamic equilibrium conditions [26] and this may have an effect on synthesis conditions when compared to either MgD<sub>2</sub> or Mg<sub>2</sub>FeD<sub>6</sub> synthesis. Rietveld analysis was used to calculate the weight fraction of each phase present together with the lattice parameters for those phases (Table 3) to compare the yield of MgD<sub>2</sub> between each batch. The highest yield of MgD<sub>2</sub> was produced from the ball milled sample; batch 4 (ca. 98%) where higher temperatures were used compared to batches 1 and 2 (400 vs 360 °C) and batch 4 was ball milled compared to batch 3. Ball milling the sample prior to absorption has been widely studied as it produces defects and imperfections that add in the transport of H, or in this case D, throughout the metal lattice [27, 28]. It appears that the longer absorption reaction times (batches 1 and 2) or increased number of desorptions (batch 1) had less of an impact on reaction conversion than higher absorption temperatures (batches 3 and 4). The Rietveld analysis showed that larger crystallite sizes were produced for MgD<sub>2</sub> as a result of

higher temperatures when compared to the changes in the aforementioned synthesis conditions.

Thermal analysis was done on batch 3 to determine the temperature at which the deuterium was released (Figure 3, fine dotted line). The onset desorption temperature above 400 °C is consistent with previously published results showing the data of unmilled  $\text{MgH}_2$  [29]. This result also indicates that thermodynamic stability of  $\text{MgD}_2$  is comparable to that of  $\text{MgH}_2$  and that the isotopic exchange does not affect desorption temperatures in the unmilled state. The TG result shows a released  $\text{D}_2$  mass that is less than the theoretical capacity of pure  $\text{MgD}_2$ . This finding is in accordance with the weight fraction calculated from the Rietveld analysis (Table 3) showing the low yield of  $\text{MgD}_2$ .

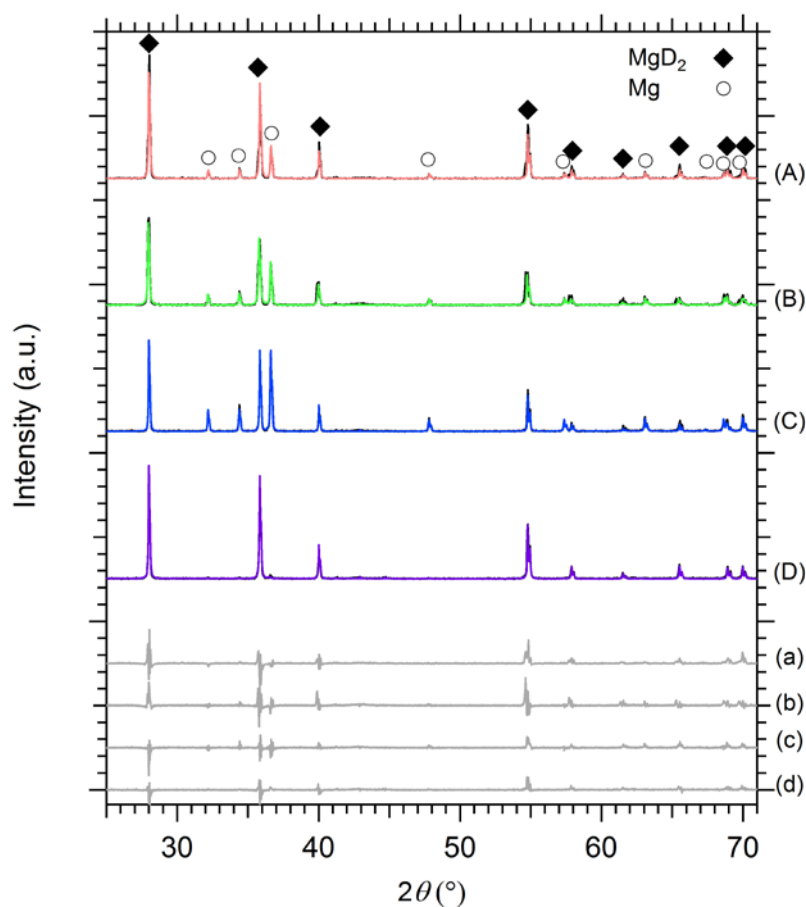


Figure 2: XRD patterns of  $\text{MgD}_2$  as a result of varying synthesis conditions (Table 1). (A)  $\text{MgD}_2$  batch 1 (B)  $\text{MgD}_2$  batch 2 (C)  $\text{MgD}_2$  batch 3 (D)  $\text{MgD}_2$  batch 4. The grey curves, (a), (b), (c), (d), show the difference in raw data (black) and the calculated Rietveld (coloured) patterns for (A), (B), (C) and (D) respectively.

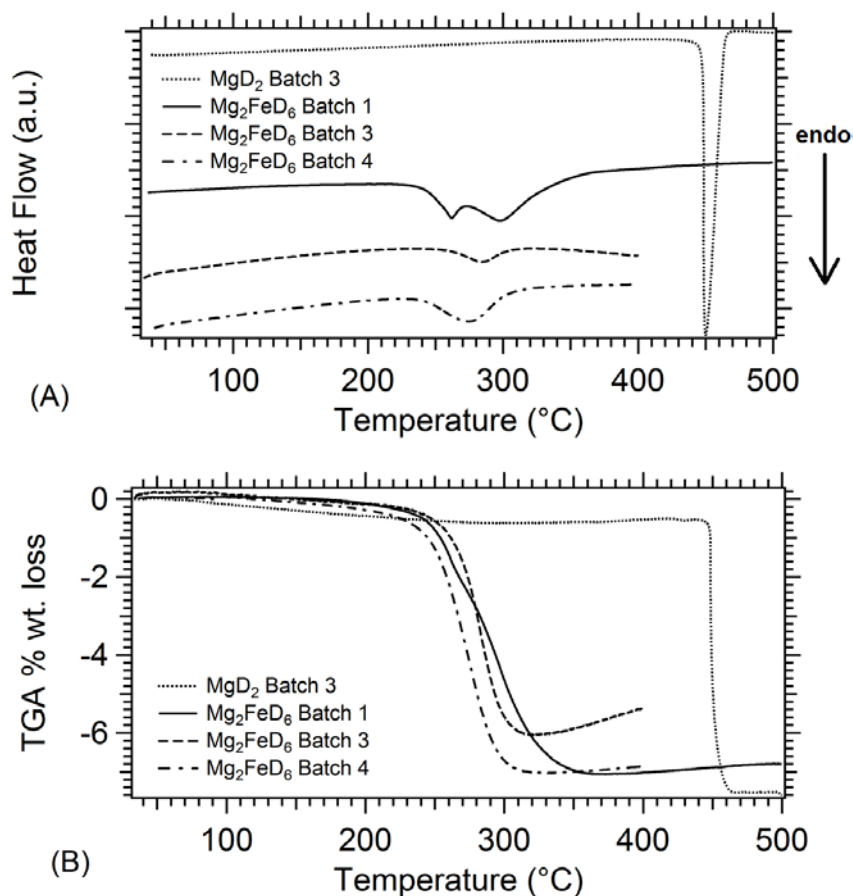


Figure 3: (A) Differential Thermal Analysis and (B) Thermogravimetric analysis of  $\text{MgD}_2$  batch 3 and  $\text{Mg}_2\text{FeD}_6$  batches 1, 3 and 4.

$\text{Mg}_2\text{FeD}_6$  synthesis was undertaken using  $\text{MgD}_2$  batches 1, 3 and 4 milled with Fe in the molar ratio of 2:1 under a  $\text{D}_2$  pressure of 10 bar (Table 2).  $\text{MgD}_2$  batch 1 was used to compare the effect of different ball to powder ratios and consequent energy transfer from the milling process to the powder to produce  $\text{Mg}_2\text{FeD}_6$  batches 1 and 2. The energy transfer was

calculated using the mathematical model developed by Burgio *et. al.* [30] and further adapted by Busch *et. al.* [31].  $\text{MgD}_2$  batches 3 and 4 were used to show the effect of deuterium concentration in the respective  $\text{MgD}_2$  samples to produce  $\text{Mg}_2\text{FeD}_6$  batches 3 and 4 respectively. Again, XRD diffractograms were obtained (Figure 4) and Rietveld analysis was used to identify and quantify the crystalline phases present in each batch and calculate the lattice parameters (Table 4). From these analyses it can be seen that different synthesis methods resulted in vastly different yields of  $\text{Mg}_2\text{FeD}_6$ .

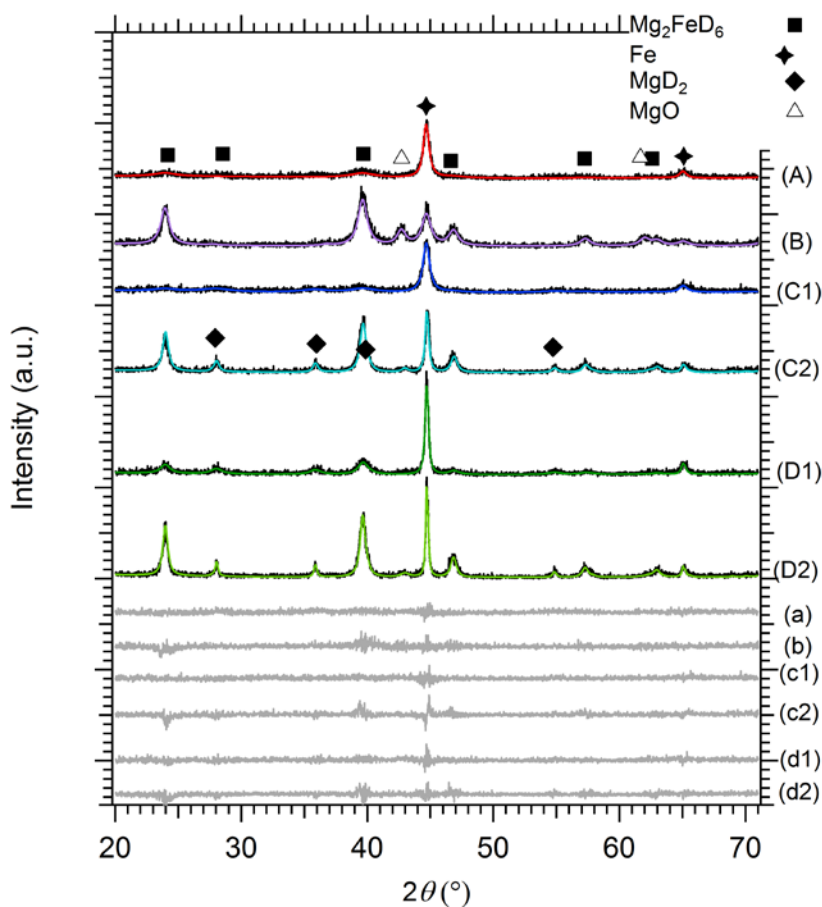


Figure 4: XRD patterns of  $\text{Mg}_2\text{FeD}_2$  as a result of varying synthesis methods (Table 2). (A)  $\text{Mg}_2\text{FeD}_2$  batch 1 (B)  $\text{Mg}_2\text{FeD}_2$  batch 2 (C1)  $\text{Mg}_2\text{FeD}_2$  batch 3 (C2)  $\text{Mg}_2\text{FeD}_2$  batch 3 further heat treated at 10 bar  $\text{D}_2$  (D1)  $\text{Mg}_2\text{FeD}_2$  batch 4 (D2)  $\text{Mg}_2\text{FeD}_2$  batch 4 further heat treated at 10 bar  $\text{D}_2$ . The grey curves, (a), (b), (c1), (c2), (d1), (d2) show the difference in raw data

(black) and the calculated Rietveld (coloured) patterns for (A), (B), (C1), (C2), (D1) and (D2) respectively.

The transferred energies for  $\text{Mg}_2\text{FeD}_6$  batches 1 and 2 were calculated to be 68.4 and 137.8 kJ/g respectively and the resultant diffractograms are given in Figure 4(A) and (B). The presence of 37 wt.%  $\text{Mg}_2\text{FeD}_6$  (Table 4) in  $\text{Mg}_2\text{FeD}_6$ -batch 1 indicates that the lower ball to powder ratio and consequent energy transfer was not enough to produce a high yield of product.  $\text{Mg}_2\text{FeD}_6$ -batch 2, on the other hand, showed a significantly increased amount of  $\text{Mg}_2\text{FeD}_6$ , however, an unexpected quantity of approximately 27 wt.% MgO (Table 2) was also present. A leak of  $\text{O}_2$  from the atmosphere during the milling process could also be a source of contamination for this batch, as a rapid pressure drop of  $\text{D}_2$  was observed and the vial reached atmospheric pressure within a couple of hours. Due to the presence of MgO, only  $\text{Mg}_2\text{FeD}_6$ -batch 1, and not batch 2, was analysed in the DTA-TG (Figure 3) and shows a much lower onset temperature ( $< 250\text{ }^\circ\text{C}$ ) compared to  $\text{MgD}_2$  in agreement with Bogdanović *et. al.* [3]. The double peak can possibly be attributed to a wide range of particle sizes produced from the low energy ball milling therefore producing heterogeneous particle and grain sizes resulting in different rates of diffusion of D out of the materials and hence the presence of two thermal events [32-34]. This double transition could also be due to the fast nucleation of  $\text{Mg}_2\text{FeD}_6$  Batch 1 as indicated by the first peak followed by slower particle growth resulting in more than one thermal transition. Another explanation could be the release of deuterium from  $\text{Mg}_2\text{FeD}_6$  closely followed by  $\beta\text{-MgD}_2$  (since there is little evidence of the  $\gamma$ - phase in the XRD data). This batch did not undergo annealing to improve the purity of the  $\text{Mg}_2\text{FeD}_6$  therefore has the lowest conversion of  $\text{MgD}_2$  to the desired product.

Table 4: Weight fraction and lattice parameter results from Rietveld Refinement of  $\text{Mg}_2\text{FeD}_6$  syntheses at 10 bar  $\text{D}_2$  pressure. As a reference, the lattice parameters provided in the Inorganic Crystal Structure Database (ICSD) are given.

Batch/Phase	Weight fraction of observed phases (%)	Lattice Parameters (Rietveld) (Å)	Lattice Parameters (ICSD) (Å)	ICSD Number
<b><math>\text{Mg}_2\text{FeD}_6</math> Batch 1</b>				
$\text{Mg}_2\text{FeD}_6$	37	a = 6.4769	a = 6.430	#29386
$\text{MgD}_2$	28	a = 4.4855, c = 3.0266	a = 4.5025, c = 3.0123	#18210
Fe	35	a = 2.8664	a = 2.8665	#53451
<b><math>\text{Mg}_2\text{FeD}_6</math> Batch 2</b>				
$\text{Mg}_2\text{FeD}_6$	56	a = 6.4341		
Fe	17	a = 2.8679		
MgO	27	a = 4.2349	a = 4.217	#9863
<b><math>\text{Mg}_2\text{FeD}_6</math> Batch 3 after annealing</b>				
$\text{Mg}_2\text{FeD}_6$	54	a = 6.4327		
$\text{MgD}_2$	21	a = 4.971, c = 3.0092		
Fe	18	a = 2.8625		
MgO	7	a = 4.2092		
<b><math>\text{Mg}_2\text{FeD}_6</math> Batch 4 after annealing</b>				
$\text{Mg}_2\text{FeD}_6$	58	a = 6.4304		
$\text{MgD}_2$	15	a = 4.4983, c = 3.0109		
Fe	17	a = 2.8640		
MgO	10	a = 4.2154		

$\text{Mg}_2\text{FeD}_6$  batches 3 and 4 produced from different purity  $\text{MgD}_2$  batches 3 and 4 were additionally annealed in low pressure  $\text{D}_2$  after reactive milling with Fe (Table 2). The same ball to powder ratio of 20:1 was used for these samples, however, using an increased milling time from 6 to 12 h. The XRD shown in Figure 4 (C1) and (D1) were measured immediately after reactive milling, prior to the annealing step. Once annealed XRD was again performed and is shown in Figure 4 (C2) and (D2). The low intensity broad peaks shown in Figure 4 (C1) and (D1) can be attributed to nano-crystallite formation of  $\text{MgD}_2$  and  $\text{Mg}_2\text{FeD}_6$  during the ball milling process. In contrast, sharper diffraction peaks after heat treatment (Figure 4

(C2) and (D2)) indicate that the crystallite sizes increased again upon annealing. The Rietveld analysis (Table 4) shows that the residual Mg in case of the lower purity starting reagents ( $\text{Mg}_2\text{FeD}_6$  batch 3) absorbed  $\text{D}_2$  and reacted to  $\text{MgD}_2$  and  $\text{Mg}_2\text{FeD}_2$ , respectively. The results show that the yield of conversion to  $\text{Mg}_2\text{FeD}_6$  does not significantly depend on the ratio  $\text{Mg}/\text{MgD}_2$  within the starting material. This is a similar result to Didisheim *et. al.* that synthesised  $\text{Mg}_2\text{FeD}_6$  from the starting reagents of elemental Mg and Fe [1] even though higher temperatures and longer reaction times were used.  $\text{Mg}_2\text{FeD}_6$  batch 4 produced a significant yield of  $\text{Mg}_2\text{FeD}_6$  (58 wt.%) higher than reported in the literature with a significantly reduced annealing time, 12 h instead of 60 h [35]. It is evident from the XRD that batch 2 underwent full conversion of  $\text{MgD}_2$  to  $\text{Mg}_2\text{FeD}_6$ , however,  $\text{O}_2$  contamination still remained an issue since MgO is thermodynamically more stable than  $\text{Mg}_2\text{FeD}_6$ . DTA-TG results from  $\text{Mg}_2\text{FeD}_6$  batches 3 and 4 are also given in Figure 3. Here the increased milling time from 6 to 12 h resulted in a more homogenous particle size compared to that of  $\text{Mg}_2\text{FeD}_6$  batch 1 resulting in a single thermal event in the DTA. The onset temperatures of  $\text{D}_2$  release remained the same around 250 °C, in agreement with the onset temperature of  $\text{H}_2$  release from  $\text{Mg}_2\text{FeH}_6$  [36]. The TG showed released amounts of deuterium of 5.8 wt.% and 6.8 wt.% for  $\text{Mg}_2\text{FeD}_6$  batches 3 and 4, respectively. These masses are in good agreement with the calculated quantities of  $\text{D}_2$  desorbed from  $\text{Mg}_2\text{FeD}_6$  according to the purities obtained by Rietveld analysis. However, this is significantly lower than the theoretical  $\text{D}_2$  capacity of 10.37 wt.% and this is most likely due to the high content of impurities including  $\text{MgD}_2$ , Fe and MgO. The difficulties in purity is not uncommon for either  $\text{Mg}_2\text{FeH}_6$  or  $\text{Mg}_2\text{FeD}_6$  with a range of synthesis methods [37-39], however, this is the first time for such high purity to be formed under 10 bar pressure.

## Conclusions

The results from this study show that  $\text{Mg}_2\text{FeD}_6$  was successfully synthesised using low pressure resulting in various yields depending on the synthesis conditions. The analysis showed that it is definitely possible to synthesise  $\text{Mg}_2\text{FeD}_6$  after both reactive ball and sintering using only a pressure of as low as 10 bar  $\text{D}_2$ .  $\text{Mg}_2\text{FeD}_6$  low pressure synthesis could be further improved by using improved seals of the milling vials and therefore preventing  $\text{O}_2$  contamination as well as increasing rounds of ball milling or reaction times in the annealing vessel whilst still keep the pressure as low as 10 bar.

## Acknowledgements

This work was partially supported by the German Federal Government under the European ERA-NET CONCERT Japan scheme via the iTHEUS project (grant CONCERT-EN-015) and the Danish Council for Strategic Research via the research project HyFillFast.

## References

- [1] Didisheim JJ, Zolliker P, Yvon K, Fischer P, Schefer J, Gubelmann M, et al. Dimagnesium iron(II) hydride,  $\text{Mg}_2\text{FeH}_6$ , containing octahedral  $\text{FeH}_6^{4-}$  anions. *Inorg Chem.* 1984;23:1953-7.
- [2] Sai Raman SS, Davidson DJ, Bobet JL, Srivastava ON. Investigations on the synthesis, structural and microstructural characterizations of Mg-based K2PtCl6 type ( $\text{Mg}_2\text{FeH}_6$ ) hydrogen storage material prepared by mechanical alloying. *J Alloys Compd.* 2002;333:282-90.
- [3] Bogdanović B, Reiser A, Schlichte K, Spliethoff B, Tesche B. Thermodynamics and dynamics of the Mg–Fe–H system and its potential for thermochemical thermal energy storage. *J Alloys Compd.* 2002;345:77-89.
- [4] Konstančuk IG, Ivanov EY, Pezat M, Darriet B, Boldyrev VV, Hagenmuller P. The hydriding properties of a mechanical alloy with composition Mg-25%Fe. *Journal of the Less Common Metals.* 1987;131:181-9.
- [5] Paskevicius M, Sheppard DA, Buckley CE. Thermodynamic changes in mechanochemically synthesized magnesium hydride nanoparticles. *J Am Chem Soc.* 2010;132:5077 – 83.
- [6] Züttel A, Wenger P, Rentsch S, Sudan P, Mauron P, Emmenegger C.  $\text{LiBH}_4$  a new hydrogen storage material. *J Power Sources.* 2003;118:1-7.
- [7] Urbanczyk R, Meggouh M, Moury R, Peinecke K, Peil S, Felderhoff M. Demonstration of  $\text{Mg}_2\text{FeH}_6$  as heat storage material at temperatures up to 550 °C. *Appl Phys A.* 2016;122:315.
- [8] Felderhoff M, Urbanczyk R, Peil S. Thermochemical heat storage for high temperature applications—a review. *Green.* 2013;3:113-23.
- [9] Paskevicius M, Sheppard DA, Williamson K, Buckley CE. Metal hydride thermal heat storage prototype for concentrating solar thermal power. *Energy.* 2015;88:469-77.

- [10] Lang J, Fritzsche H, Asselli AAC, Huot J. In-situ neutron diffraction investigation of Mg<sub>2</sub>FeH<sub>6</sub> dehydrogenation. *Int J Hydrogen Energy*. 2016.
- [11] Deng S, Xiao X, Han L, Li Y, Li S, Ge H, et al. Hydrogen storage performance of 5LiBH<sub>4</sub> + Mg<sub>2</sub>FeH<sub>6</sub> composite system. *Int J Hydrogen Energy*. 2012;37:6733-40.
- [12] Ghaani MR, Catti M, Nale A. Thermodynamics of Dehydrogenation of the 2LiBH<sub>4</sub>-Mg<sub>2</sub>FeH<sub>6</sub> Composite. *The Journal of Physical Chemistry C*. 2012;116:26694-9.
- [13] Puzskiel J, Gennari F, Larochette PA, Karimi F, Pistidda C, Gosalawit-Utke R, et al. Sorption behavior of the MgH<sub>2</sub>-Mg<sub>2</sub>FeH<sub>6</sub> hydride storage system synthesized by mechanical milling followed by sintering. *Int J Hydrogen Energy*. 2013;38:14618-30.
- [14] Puzskiel JA, Arneodo Larochette P, Gennari FC. Thermodynamic-kinetic characterization of the synthesized Mg<sub>2</sub>FeH<sub>6</sub>-MgH<sub>2</sub> hydrides mixture. *Int J Hydrogen Energy*. 2008;33:3555-60.
- [15] Chaudhary A-L, Li G, Matsuo M, Orimo S-i, Deledda S, Sørby MH, et al. Simultaneous desorption behavior of M borohydrides and Mg<sub>2</sub>FeH<sub>6</sub> reactive hydride composites (M = Mg, then Li, Na, K, Ca). *Appl Phys Lett*. 2015;107:073905.
- [16] Li G, Matsuo M, Deledda S, Hauback BC, Orimo S. Dehydrogenating Property of NaBH<sub>4</sub> Combined with Mg<sub>2</sub>FeH<sub>6</sub>. *Materials Transactions*. 2014;55:1141-3.
- [17] Li G, Matsuo M, Deledda S, Sato R, Hauback BC, Orimo S. Dehydrogenating Properties of LiBH<sub>4</sub> Combined with Mg<sub>2</sub>FeH<sub>6</sub>. *Materials Transactions*. 2013;54:1532 - 4.
- [18] Li G, Matsuo M, Aoki K, Ikeshoji T, Orimo S-i. Dehydrogenating Process and Hydrogen-Deuterium Exchange of LiBH<sub>4</sub>-Mg<sub>2</sub>FeH<sub>6</sub> Composites. *Energies*. 2015;8:5459.
- [19] Herrich M, Ismail N, Lyubina J, Handstein A, Pratt A, Gutfleisch O. Synthesis and decomposition of Mg<sub>2</sub>FeH<sub>6</sub> prepared by reactive milling. *Materials Science and Engineering: B*. 2004;108:28-32.
- [20] Polanski M, Nielsen TK, Cerenius Y, Bystrzycki J, Jensen TR. Synthesis and decomposition mechanisms of Mg<sub>2</sub>FeH<sub>6</sub> studied by in-situ synchrotron X-ray diffraction and high-pressure DSC. *Int J Hydrogen Energy*. 2010;35:3578-82.
- [21] Polanski M, Płociński T, Kuncce I, Bystrzycki J. Dynamic synthesis of ternary Mg<sub>2</sub>FeH<sub>6</sub>. *Int J Hydrogen Energy*. 2010;35:1257-66.
- [22] Huot J, Hayakawa H, Akiba E. Preparation of the hydrides Mg<sub>2</sub>FeH<sub>6</sub> and Mg<sub>2</sub>CoH<sub>5</sub> by mechanical alloying followed by sintering. *J Alloys Compd*. 1997;248:164-7.
- [23] Varin RA, Li S, Calka A, Wexler D. Formation and environmental stability of nanocrystalline and amorphous hydrides in the 2Mg-Fe mixture processed by controlled reactive mechanical alloying (CRMA). *J Alloys Compd*. 2004;373:270-86.
- [24] Gennari FC, Castro FJ, Andrade Gamboa JJ. Synthesis of Mg<sub>2</sub>FeH<sub>6</sub> by reactive mechanical alloying: formation and decomposition properties. *J Alloys Compd*. 2002;339:261-7.
- [25] Puzskiel J, Larochette PA, Gennari F. Thermodynamic and kinetic studies of Mg-Fe-H after mechanical milling followed by sintering. *J Alloys Compd*. 2008;463:134-42.
- [26] Paskevicius M, Sheppard DA, Chaudhary AL, Webb CJ, Gray EMA, Tian HY, et al. Kinetic limitations in the Mg-Si-H system. *Int J Hydrogen Energy*. 2011;36:10779-86.
- [27] Dornheim M, Doppiu S, Barkhordarian G, Boesenberg U, Klassen T, Gutfleisch O, et al. Hydrogen storage in magnesium-based hydrides and hydride composites. *Scripta Mater*. 2007;56:841-6.
- [28] Dornheim M, Eigen N, Barkhordarian G, Klassen T, Bormann R. Tailoring hydrogen storage materials towards application. *Adv Eng Mater*. 2006;8:377 - 85.
- [29] Imamura H, Masanari K, Kusuhara M, Katsumoto H, Sumi T, Sakata Y. High hydrogen storage capacity of nanosized magnesium synthesized by high energy ball-milling. *J Alloys Compd*. 2005;386:211-6.
- [30] Burgio N, Iasonna A, Magini M, Martelli S, Padella F. Mechanical alloying of the Fe-Zr system. Correlation between input energy and end products. *Il nuovo cemento D*. 1991;13:459-76.
- [31] Busch N, Jepsen J, Pistidda C, Puzskiel JA, Karimi F, Milanese C, et al. Influence of milling parameters on the sorption properties of the LiH-MgB<sub>2</sub> system doped with TiCl<sub>3</sub>. *J Alloys Compd*. 2015;645:S299-S303.

- [32] Chaudhary A-L, Paskevicius M, Sheppard DA, Buckley CE. Thermodynamic destabilisation of  $MgH_2$  and  $NaMgH_3$  using Group IV elements Si, Ge or Sn. *J Alloys Compd.* 2015;623:109-16.
- [33] Varin RA, Czujko T, Wronski Z. Particle size, grain size and  $\gamma$ -MgH<sub>2</sub> effects on the desorption properties of nanocrystalline commercial magnesium hydride processed by controlled mechanical milling. *Nanotechnology.* 2006;17:3856.
- [34] Chaudhary A-L, Sheppard DA, Paskevicius M, Pistidda C, Dornheim M, Buckley CE. Reaction kinetic behaviour with relation to crystallite/grain size dependency in the Mg–Si–H system. *Acta Mater.* 2015;95:244-53.
- [35] Huot J, Boily S, Akiba E, Schulz R. Direct synthesis of  $Mg_2FeH_6$  by mechanical alloying. *J Alloys Compd.* 1998;280:306-9.
- [36] Callini E, Aguey-Zinsou K-F, Ahuja R, Ares JR, Bals S, Biliškov N, et al. Nanostructured materials for solid-state hydrogen storage: A review of the achievement of COST Action MP1103. *Int J Hydrogen Energy.* 2016.
- [37] Shang CX, Bououdina M, Guo ZX. Direct mechanical synthesis and characterisation of  $Mg_2Fe(Cu)H_6$ . *J Alloys Compd.* 2003;356–357:626-9.
- [38] Li S, Varin RA, Morozova O, Khomenko T. Controlled mechano-chemical synthesis of nanostructured ternary complex hydride  $Mg_2FeH_6$  under low-energy impact mode with and without pre-milling. *J Alloys Compd.* 2004;384:231-48.
- [39] Castro FJ, Gennari FC. Effect of the nature of the starting materials on the formation of  $Mg_2FeH_6$ . *J Alloys Compd.* 2004;375:292-6.